Abstracta

Ano XXIV - N. 02

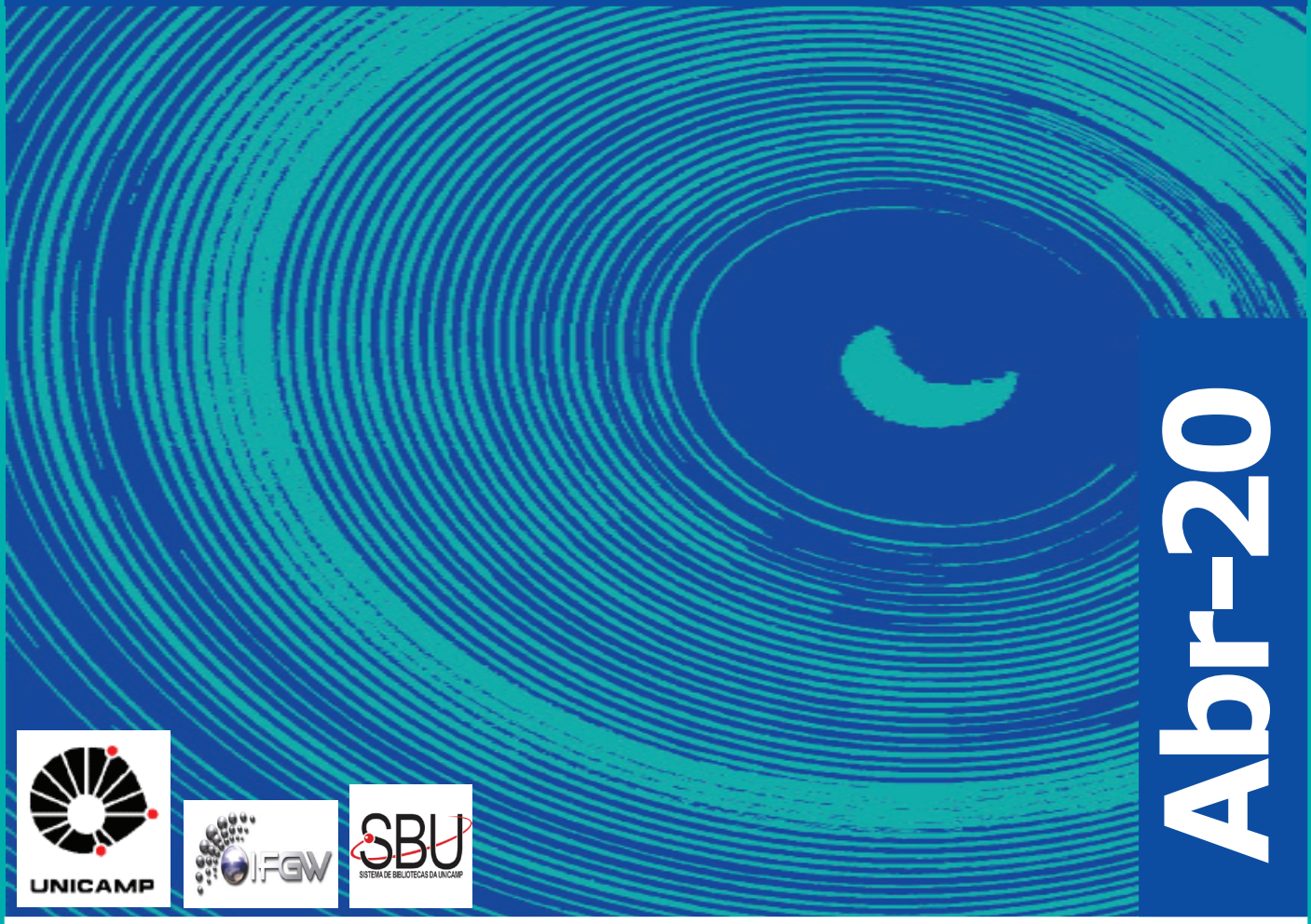

Abr-20

Artigos publicados 2020 - P017-2020 à P084-2020

Evenos publicados 2019 - P001-2019 à P002-2019

Defesas de Dissertações do IFGW - D003-2020 à D006-2020

Defesas de Teses do IFGW - T003-2020 à T006-2020

Defesas de Teses e Dissertações do PECIM - P001-2020

Artigos publicados 2020

[P017-2020] "All-Optical Fiber Anemometer Based on the Pitot-Static Tube"

Fujiwara, E.; **Delfino, T. D.*; Cabral, T. D.*; Cordeiro, C. M. D.***

An optical fiber anemometer based on the Pitot-static tube is reported. The device was fabricated in a 3-D printer, and the pressure difference was assessed by means of a latex rubber diaphragm with a mounted fiber Bragg grating probe, so the membrane deflection is obtained in terms of the fiber curvature. The sensor characteristics were first obtained by the simulation in order to determine the correlation between the Bragg wavelength shifts and the airflow speed. Next, the device was experimentally evaluated in a wind tunnel, allowing for the assessment of a 20-36-m/s dynamic range, with 24.9-pm/(m/s) maximum sensitivity and 0.04-m/s resolution. Finally, the system was tested on the measurement of cyclic airflow speeds for predicting the applied speed according to the calibration curve, yielding reproducible results with an average error of 0.98 m/s, which is comparable to other reported sensors based on more complex designs and interrogation setups.

IEEE TRANSACTIONS ON INSTRUMENTATION AND MEASUREMENT 69[4], 1805-1811, Parte: 2, 2020. DOI: 10.1109/TIM.2019.2915392

[P018-2020] "Anisotropic lattice compression and pressure--induced electronic phase transitions in Sr2IrO4"

Samanta, K.*; Tartaglia, R.*; Kaneko, U. F.; Souza-Neto, N. M.; **Granado, E.***

The crystal lattice of Sr2IrO4 is investigated with synchrotron x-ray powder diffraction under hydrostatic pressures up to P = 43 GPa and temperatures down to 20 K. The tetragonal unit cell is maintained over the whole investigated pressure range, within our resolution and sensitivity. The c-axis compressibility kappa(c)(P, T) -(1/c)(dc/dP) presents an anomaly with pressure at P-1 = 17 GPa at fixed T = 20 K that is not observed at T = 300 K, whereas kappa(a)(P, T) is nearly temperature independent and shows a linear behavior with P. The anomaly in kappa(c)(P, T) is associated with the onset of long-range magnetic order, as evidenced by an analysis of the temperature dependence of the lattice parameters at fixed P = 13.7 +/- 0.5 GPa. the collapse of the J(eff) = 1/2 spin-orbit-entangled state. Our results support pressure-induced phase transitions or crossovers between electronic ground states that are sensed, and therefore can be probed, by the crystal lattice at low temperatures in this prototype spin-orbit Mott insulator.

PHYSICAL REVIEW B [7], 07512, 2020. DOI: 10.1103/PhysRevB.101.075121

[P019-2020] "Ar/Cl-2 etching of GaAs optomechanical microdisks fabricated with positive electroresist"

Benevides, R.*; Menard, M.; **Wiederhecker, G. S.*; Alegre, T. P. M.***

A method to fabricate GaAs microcavities using only a soft mask with an electrolithographic pattern in an inductively coupled plasma etching is presented. A careful characterization of the fabrication process pinpointing the main routes for a smooth device sidewall is discussed. Using the final recipe, optomechanical microdisk resonators are fabricated. The results show very high optical quality factors of Q(opt) > 2 x 10(5), among the largest already reported for dry-etching devices. The final devices are also shown to present high mechanical quality factors and an optomechanical vacuum coupling constant of g(0) = 2 pi x 13.6 kHz enabling self-sustainable mechanical oscillations for an optical input power above 1 mW.

OPTICAL MATERIALS EXPRESS 10[1], 57-67, 2020. DOI: 10.1364/OME.10.000057

[P020-2020] "Binary activated iron oxide/SiO2/NaGdF4:RE (RE = Ce, and Eu; Yb, and Er) nanoparticles: synthesis, characterization and their potential for dual T-1-T-2 weighted imaging"

Shrivastava, N.; Garcia, J.; Rocha, U.; Ospina, C.; **Muraca, D.*;** de Menezes, A. S.; Jacinto, C.; Louie, A. Y.; Zoppellaro, G.; Sharma, S. K.

We report the microwave-assisted synthesis of binary doped optical-magnetic up/downconverting NaGdF4:RE and iron oxide/SiO2/NaGdF4:RE nanoparticles. The morphological characteristics were finely tuned from elongated rod-shaped to ovoidal nanoparticles. The (Yb, and Er) activated particles provided an excellent up/down conversion luminescence emission in the green and mid-infrared region under excitation of 980 nm, whereas the (Ce, and Eu) activated systems exhibited a strong red emission via the Gd3+ sublattice upon excitation in the UV region. The magnetic hysteresis at 300 K for beta-NaGdF4:RE showed typical signatures of a paramagnetic system, whereas iron oxide/SiO2/beta-NaGdF4:RE exhibited superparamagnetic behavior along with a Curie-like component. The luminescence quenching effects induced by the presence of iron oxide phase have been validated through comparing the emission/lifetime decay curves. In addition to the excellent optical and magnetic properties, these materials show remarkably high longitudal and transverse relaxivity values (for Fe and Gd) and thus are potential candidates for T-1 and T-2-weighted bioimaging.

NEW JOURNAL OF CHEMISTRY 44[3], 832-844, 2020. DOI: 10.1039/c9nj03929e

[P021-2020] "Bioinspired Aluminum Composite Reinforced with Soft Polymers with Enhanced Strength and Plasticity"

Rout, A.; Gumaste, A.; Pandey, P.; **Oliveira, E. F.***; Demiss, S.; Mahesh, V. P.; Bhatt, C.; Raphael, K.; Ayyagari, R. S.; Autreto, P. A. S.; Palit, M.; Olu, F.; **Galvao, D. S.***; Arora, A.; Tiwary, C. S.

Composites have played a key role in revolutionizing the automobile, marine, and aerospace industries. There is a constant attempt for the development of low-density composite materials with superior mechanical and corrosion-resistant properties for elevated temperature applications. Herein, an attempt is made to develop a nature-inspired unique aluminum-based composite with low-density polymer (polyethylene terephthalate, i.e., soft material) reinforcement, which shows an enhancement in strength and toughness. The composite is processed using the easily scalable and simple friction stir processing technique. Mechanical properties of the uniformly reinforced aluminum composite show double ultimate strength and fivefold improvement in plasticity. The ultimate strength of the composite increases at elevated temperatures. The experimental observations are further supported by theoretical calculations and molecular dynamics simulations.

ADVANCED ENGINEERING MATERIALS 22[3], 1901116, 2020. DOI: 10.1002/adem.201901116

[P022-2020] "Bose-Einstein correlations of charged hadrons in proton-proton collisions at √s = 13 TeV"

Sirunyany, A. M.; Tumasyan, A.; Adam, W.; **Chinellato, J. A.*; Tonelli Manganote, E. J.***; et al.; CMS Collaboration

Bose-Einstein correlations of charged hadrons are measured over a broad multiplicity range, from a few particles up to about 250 reconstructed charged hadrons in proton-proton collisions at <mml:msqrt>s</mml:msqrt> = 13 TeV. The results are based on data collected using the CMS detector at the LHC during runs with a special low-pileup configuration. Three analysis techniques with different degrees of dependence on simulations are used to remove the non-Bose-Einstein background from the correlation functions. All three methods give consistent results. The measured lengths of homogeneity are studied as functions of particle multiplicity as well as average pair transverse momentum and mass. The results are compared with data from both CMS and ATLAS at <mml:msqrt>s</mml:msqrt> = 7 TeV, as well as with theoretical predictions.

JOURNAL OF HIGH ENERGY PHYSICS [3], 2020. DOI: 10.1007/JHEP03(2020)014

[P023-2020] "Boundary conditions and vacuum fluctuations in AdS(4)"

Barroso, V. S.*; Pitelli, J. P. M.

Initial conditions given on a spacelike, static slice of a non-globally hyperbolic spacetime may not define the fates of classical and quantum fields uniquely. Such lack of global hyperbolicity is a well-known property of the anti-de Sitter solution and led many authors to question how is it possible to develop a quantum field theory on this spacetime. Wald and Ishibashi took a step towards the healing of that causal issue when considering the propagation of scalar fields on AdS. They proposed a systematic procedure to obtain a physically consistent dynamical evolution. Their prescription relies on determining the self-adjoint extensions of the spatial component of the differential wave operator. Such a requirement leads to the imposition of a specific set of boundary conditions at infinity. We employ their scheme in the particular case of the four-dimensional AdS spacetime and compute the expectation values of the field squared and the energy-momentum tensor, which will then bear the effects of those boundary conditions. We are not aware of any laws of nature constraining us to prescribe the same boundary conditions to all modes of the wave equation. Thus, we formulate a physical setup in which one of those modes satisfy a Robin boundary condition, while all others satisfy the Dirichlet condition. Due to our unusual settings, the resulting contributions to the fluctuations of the expectation values will not respect AdS invariance. As a consequence, a back-reaction procedure would yield a non-maximally symmetric spacetime. Furthermore, we verify the violation of weak energy condition as a direct consequence of our prescription for dynamics.

GENERAL RELATIVITY AND GRAVITATION 52[3], 29, 2020. DOI: 10.1007/s10714-020-02672-4

[P024-2020] "Bright and Vivid Diffractive-Plasmonic Reflective Filters for Color Generation"

Melo, E. G.*; Ribeiro, A. L. A.*; Benevides, R. S.*; Zuben, A. A. G. V.*; dos Santos, M. V. P.*; Silva, A. A.; **Wiederhecker, G. S.*; Alegre, T. P. M.***

The desire to reproduce vivid colors such as those found in birds, fishes, flowers, and insects has driven extensive research into nanostructured surfaces especially because of their high spatial resolution. Using a periodic silicon-patterned structure coated with aluminum, we combine two distinct and yet interconnected effects to produce bright and vivid color surfaces. A genetic algorithm optimization process was used to fine-tune both the diffraction and plasmonic effects to obtain reflective color filters for the red, green, and blue colors. The obtained structures are suitable for displays, image applications, color sensors, and optical filters.

ACS APPLIED NANO MATERIALS 3[2], 1111-1117, 2020. DOI: 10.1021/acsanm.9b02508

[P025-2020] "Calorimetry for low-energy electrons using charge and light in liquid argon"

Foreman, W.; Acciarri, R.; Asaadi, J. A.; **Machado, A. A. B.*; Segreto, E.***; et al.; LArIAT Collaboration

Precise calorimetric reconstruction of 5-50 MeV electrons in liquid argon time projection chambers (LArTPCs) will enable the study of astrophysical neutrinos in DUNE and could enhance the physics reach of oscillation analyses. Liquid argon scintillation light has the potential to improve energy reconstruction for low-energy electrons over charge-based measurements alone. Here we demonstrate light-augmented calorimetry for low-energy electrons in a single-phase LArTPC using a sample of Michel electrons from decays of stopping cosmic muons in the LArIAT experiment at Fermilab. Michel electron energy spectra are reconstructed using both a traditional charge-based approach as well as a more holistic approach that incorporates both charge and light. A maximum-likelihood fitter, using LArIAT's well-tuned simulation, is developed for combining these quantities to achieve optimal energy resolution. A sample of isolated electrons is simulated to better determine the energy resolution expected for astrophysical electron-neutrino charged-current interaction final states. In LArIAT, which has very low wire noise and an average light yield of 18 pe/MeV, an energy resolution of sigma/E similar or equal to 9.3%/root E circle plus 1.3% is achieved. Samples are then generated with varying wire noise levels and light yields to gauge the impact of light-augmented calorimetry in larger LArTPCs. At a charge-readout signal-to-noise of S/N similar or equal to 30, for example, the energy resolution for electrons below 40 MeV is improved by 10%, approximate to 120%, and approximate to 40% over charge-only calorimetry for average light yields of 10 pe/MeV, 20 pe/MeV, and 100 pe/MeV, respectively.

PHYSICAL REVIEW D 101[1], 012010, 2020. DOI: 10.1103/PhysRevD.101.012010

[P026-2020] "Compatibility of linear-response theory with the second law of thermodynamics and the emergence of negative entropy production rates"

Naze, P.*; Bonanca, M. V. S.*

The reliability of physical theories depends on whether they agree with well-established physical laws. In this work, we address the compatibility of the Hamiltonian formulation of linear-response theory with the second law of thermodynamics. In order to do so, we verify three complementary aspects often understood as statements of the second law: (1) no dissipation for quasistatic process; (2) dissipation for finite-time processes; and (3) positive entropy production rate. Our analysis focuses on two classes of nonequilibrium isothermal processes: slowly-varying and finite-time but weak ones. For the former, we show that these aspects are easily verified. For the later, we present conditions for the achievement of the first two aspects. We also show that the third one is not always verified, presenting an example based on Brownian motion in which we observe negative values in the entropy production rate. In particular, we compare linear-response and exact results for this example.

JOURNAL OF STATISTICAL MECHANICS-THEORY AND EXPERIMENT 2020[1], 013206, 2020. DOI: 10.1088/1742-5468/ab54ba

[P027-2020] "Cyano-Functionalized Porphyrins on Cu(111) from One-Dimensional Wires to Two-Dimensional Molecular Frameworks: On the Role of Co-Deposited Metal Atoms"

dos Santos, A. C.*; Ferreira, R. C. D.*; Moreno-Lopez, J. C.; Barreto, L.; Lepper, M.; **Landers, R.***; Steinruck, H. P.; Marbach, H.; **de Siervo, A.***

Metal adatoms play a key role in surface diffusion, adsorption conformation, and self-assembly of porphyrin molecules on metal surfaces. Herein, we study the specific influence of coadsorption of Fe, Co, and Pd atoms on the behavior of 2H--tetiakis(p-cyano)phenylporphyrin (2H-TCNPP) on Cu(111) using scanning tunneling microscopy. Upon codeposition of Fe and Co, the molecules form one-dimensional (1D) linear chains after mild annealing on Cu(111) driven by the interaction of its cyano groups with metal adatoms. A similar behavior has been observed previously on Cu(111), mediated by Cu adatoms, where the functional CN groups were also found to lower the reaction rate of the so-called porphyrin self-metalation reaction with Cu atoms significantly, in comparison to the non--cyano-functionalized porphyrin. Upon co-deposition of Pd and mild annealing, we find a remarkably different behavior, that is, a massive reorganization from 1D molecular chains to a peculiar rectangular 2D (two-dimensional) network. The molecular appearance changes to a clover shape, which is attributed to a Pd-induced dehydrogenation and subsequent ring closure reaction of the phenyl and pyrrole groups.

CHEMISTRY OF MATERIALS 32[5], 2114-2122, 2020. DOI: 10.1021/acs.chemmater.9b05256

[P028-2020] "Density-functional theory prediction of the elastic constants of ice I-h"

Rego, J. S.*; de Koning, M.*

We assess the elastic stiffness constants of hexagonal proton--disordered ice I-h as described by density-functional theory calculations. Specifically, we compare the results for a set of nine exchange-correlation functionals, including standard generalized-gradient approximations (GGAs), the strongly constrained and appropriately normed (SCAN) metaGGA functional, and a number of dispersion-corrected versions based on the van der Waals (vdW) and VV10 schemes. Compared to the experimental data, all functionals predict an excessively stiff response to tensile and compressive distortions, as well as shear deformations along the basal plane, with the SCAN metaGGA functional displaying the largest deviations as compared to the experimental values. These discrepancies are found to correlate with underestimates of inter-molecular distances, on the one hand, and overestimates of intra-molecular separations, on the other. The inclusion of non-local vdW corrections according to the vdW approach generally improves these structural parameters and softens the elastic response functions compared to their parent GGA functionals. The dispersion-corrected SCAN-rVV10 functional, however, acts in the opposite direction, further worsening the comparison to experiment. In this view, it appears useful that the database employed to gauge the quality of exchange-correlation functionals for water includes an assessment of their elastic response of ice I-h and possibly other crystalline phases.

JOURNAL OF CHEMICAL PHYSICS 152[8], 084502, 2020. DOI: 10.1063/1.5142710

[P029-2020] "Detection of Cross-Correlation between Gravitational Lensing and gamma Rays"

Ammazzalorso, S.; Gruen, D.; **Sobreira, F.***; et al.

In recent years, many gamma-ray sources have been identified, yet the unresolved component hosts valuable information on the faintest emission. In order to extract it, a cross-correlation with gravitational tracers of matter in the Universe has been shown to be a promising tool. We report here the first identification of a cross-correlation signal between gamma rays and the distribution of mass in the Universe probed by weak gravitational lensing. We use data from the Dark Energy Survey Y1 weak lensing data and the Fermi Large Area Telescope 9-yr gamma--ray data, obtaining a signal-to-noise ratio of 5.3. The signal is mostly localized at small angular scales and high gamma-ray energies, with a hint of correlation at extended separation. Blazar emission is likely the origin of the small-scale effect. We investigate implications of the large-scale component in terms of astrophysical sources and particle dark matter emission.

PHYSICAL REVIEW LETTERS 124[10], 101102, 2020. DOI: 10.1103/PhysRevLett.124.101102

[P030-2020] "Determination of fast neutron RBE using a fully mechanistic computational model"

Zabihi, A.; **Tello, J.***; Incerti, S.; Francis, Z.; Forozani, G.; Semsarha, F.; Moslehi, A.; **Bernal, M. A.***

This work presents a model previously developed for estimating relative biological effectiveness (RBE) associated with high-LET particles. It is based on the combination of Monte Carlo simulations of particle interactions when traversing an atomic resolution DNA geometrical model. In addition, the model emulates the induction of lethal damage from the interaction of two sublethal lesions, taken as double-strand breaks. The Geant4--DNA package was used for simulations with liquid water as the transport medium. The RBE of neutron beams with energies ranging from 0.1 MeV up to 14 MeV was studied. The model succeeded in reproducing the general behavior of RBE as a function of neutron energy, including the RBE peak reported by experiments at approximately 0.4 MeV. Furthermore, the results of the model agree rather well with some experimental works. However, our results underestimate RBE for neutron energies above approximately 5 MeV due to the current limitations of Geant4-DNA for the tracking of heavy ions below 0.5 MeV/u.

APPLIED RADIATION AND ISOTOPES 156, UNSP 108952, 2020. DOI: 10.1016/j.apradiso.2019.108952

[P031-2020] "Dielectric Permittivity and Surface Charge Density in Layer-by-Layer Poly(diallyldimethylammonium chloride)/Poly(styrenesulfonate) Nanostructured Films: Implications for Biosensing"

Hensel, R. C.*; Pereira-da-Silva, M. A.; **Riul, A.*; Rodrigues, V.***

The development of sensors based on nanostructures is an important task in fundamental and applied sciences to increase their sensitivity and selectivity. A better comprehension of materials aggregation at the nanoscale can provide insights and innovations for sensing and electronic appliances. We analyzed the electrical properties of polyelectrolytes assembled in a multilayered architecture with nanometric thickness control. We have fabricated layer-by-layer (LbL) thin films alternating positively charged poly(diallyldimethylammonium chloride) (PDDA) and negatively charged poly-(styrenesulfonate) (PSS) in a PDDA/PSS architecture. A homemade setup tracked the nanostructure growth by measuring the capacitance after each deposited layer onto gold interdigitated electrodes (IDEs). The capacitance increase linearly after each adsorbed bilayer, which is associated with the dielectric layer accumulated onto the IDEs. We interpreted such behavior in terms of the electrostatic potential on the IDEs, resulting in a dielectric constant of 21 +/- 3 for the PDDA/PSS film.

Furthermore, we observed the capacitance changing in a zigzag-like behavior according to the outermost deposited layer due to the charge reversal process. Polycation surface charge density was estimated as (5.8 +/- 0.2) x 10(-20) c/mu m(2). We also analyzed the strong and weak character of PDDA and poly(allylamine hydrochloride) (PAH). The methodology proposed here allows for a better material choice that best suits a particular LbL application. Besides, the quantitative evaluation of the outermost layer charge density should enhance the adsorption of molecules that are routinely employed as active layers in (bio)sensing applications, contributing to improvements in (bio)sensor engineering.

ACS APPLIED NANO MATERIALS 3[2], 1749-1754, 2020. DOI: 10.1021/acsanm.9b02447

[P032-2020] "Dynamical Classification of Trans-Neptunian Objects Detected by the Dark Energy Survey"

Khain, T.; Becker, J. C.; Lin, H. W. **Sobreira, F.***; et al.; Dark Energy Survey Collaboration

The outer solar system contains a large number of small bodies (known as trans-Neptunian objects or TNOs) that exhibit diverse types of dynamical behavior. The classification of bodies in this distant region into dynamical classes-subpopulations that experience similar orbital evolution-aids in our understanding of the structure and formation of the solar system. In this work, we propose an updated dynamical classification scheme for the outer solar system. This approach includes the construction of a new (automated) method for identifying mean motion resonances. We apply this algorithm to the current data set of TNOs observed by the Dark Energy Survey (DES) and present a working classification for all of the DES TNOs detected to date. Our classification scheme yields 1 inner centaur, 19 outer centaurs, 21 scattering disk objects, 47 detached TNOs, 48 securely resonant objects, 7 resonant candidates, and 97 classical belt objects. Among the scattering and detached objects, we detect 8 TNOs with semimajor axes greater than 150 au.

ASTRONOMICAL JOURNAL 159[4], 133, 2020. DOI: 10.3847/1538-3881/ab7002

[P033-2020] "Effect of the period of the substrate oscillation in the dynamic glancing angle deposition technique: A columnar periodic nanostructure formation"

Jimenez, M. J. M.*; Antunes, V. G.*; Zagonel, L. F.*; Figueroa, C. A.; **Wisnivesky, D.*; Alvarez, F.***

Nanostructured CrN thin films are obtained by combining RF physical vapor and dynamic glancing angle deposition using a computer-controlled substrate oscillatory motion. By using an appropriate frequency for substrate oscillation, it becomes feasible to tailor the physical properties of thin films deposited onto the substrate. The films are deposited by moving the substrate back and forward between specified angles with, among other parameters, a controlled time-dependent angular position phi(t) of the substrate. Thus, the direction of atoms striking the film changes in accordance to the position of the substrate. In this paper, we report the physical properties of a material for a varying frequency of substrate oscillation while maintaining the same angular phi(t) function (triangular function) in all the studied samples. By controlling the incidence angle phi(t) for precursor atoms impinging upon the substrate, one can prompt the formation of wavy-like periodic columnar nanostructures. The physical characteristics of the coating such as morphology, residual stress, nanohardness, crystallite size, composition, and texture of the columnar periodic multistructured films are all remarkably dependent on the oscillation frequency. The cited physical properties obtained by moving the substrate forward and back with an angular phi(t) triangular function and several periods of oscillation are reported and analyzed.

SURFACE & COATINGS TECHNOLOGY 383, 125237, 2020. DOI: 10.1016/j.surfcoat.2019.125237

[P034-2020] "Effective field theory interactions for liquid argon target in DarkSide-50 experiment"

Agnes, P.; Albuquerque, I. F. M.; Alexander, T.; **Machado, A. A.*; Segreto, E.***; et al.; DarkSide-50 Collaboration

We reanalyze data collected with the DarkSide-50 experiment and recently used to set limits on the spin-independent interaction rate of weakly interacting massive particles (WIMPs) on argon nuclei with an effective field theory framework. The dataset corresponds to a total (16660 +/- 270) kg d exposure using a target of low-radioactivity argon extracted from underground sources. We obtain upper limits on the effective couplings of the 12 leading operators in the nonrelativistic systematic expansion. For each effective coupling we set constraints on WIMP-nucleon cross sections, setting upper limits between 2.4 x 10(-45) cm(2) and 2.3 x 10(-42) cm(2) (8.9 x 10(-45) cm(2) and 6.0 x 10(-)(42) cm(2)) for WIMPs of mass of 100 GeV/c(2) (1000 GeV/c(2)) at 90% confidence level.

PHYSICAL REVIEW D 101[6], 062002, 2020. DOI: 10.1103/PhysRevD.101.062002

[P035-2020] "Electrical contact resistance and tribological behaviors of self-lubricated dielectric coating under different conditions"

Echeverrigaray, F. G.*; de Mello, S. R. S.*; Leidens, L. M.; Boeira, C. D.; Michels, A. F.; Braceras, I.; Figueroa, C. A.

In this study, the electro-tribological performance of hydrogenated amorphous carbon coatings against bearing steel in different experimental conditions was continuously monitored by means of coefficient of friction (CoF) and electrical contact resistance (ECR). The influence of tribosystem variables such as humidity, velocity and lifetime on frictional and electrical response were also compared with specific wear energy calculation method. The main findings of both tribological and electrical behaviors include the dissipated energy and the micro-slip dielectric failures that can be linked to the properties of self-lubricating layers, which depend also on the working media. In this framework, the electro-tribological evaluation provides an electrical monitoring tool for coating premature wear detection in real time.

TRIBOLOGY INTERNATIONAL 143, 106086, 2020. DOI: 10.1016/j.triboint.2019.106086

[P036-2020] "Emergent SU(N) symmetry in disordered SO(N) spin chains"

Quito, V. L.; Lopes, P. L. S.; Hoyos, J. A.; **Miranda, E.***

Strongly disordered spin chains invariant under the SO(N) group are shown to display random-singlet phases with emergent SU(N) symmetry without fine tuning. The phases with emergent SU(N) symmetry are of two kinds: one has a ground state formed of randomly distributed singlets of strongly bound pairs of SO(N) spins (a 'mesonic' phase), while the other has a ground state composed of singlets made out of strongly bound integer multiples of N SO(N) spins (a 'baryonic' phase).

The established mechanism is general and we put forward the cases of N = 2, 3, 4 and 6 as prime candidates for experimental realizations in material compounds and cold-atoms systems. We display universal temperature scaling and critical exponents for susceptibilities distinguishing these phases and characterizing the enlarging of the microscopic symmetries at low energies.

EUROPEAN PHYSICAL JOURNAL B 93[1], 17, 2020. DOI: 10.1140/epjb/e2019-100576-6

[P037-2020] "Energy barriers for collapsing large-diameter carbon nanotubes"

Del Grande, R. R.; **Fonseca, A. F.***; Capaz, R. B.

Single-wall carbon nanotubes (SWNTs) are best known in their hollow cylindrical shapes, but the ground state of large-diameter tubes actually corresponds to a collapsed dumbbell-like structure, where the opposite sides of the nanotube wall are brought in contact and stabilized by van der Waals attraction. For those tubes, the cylindrical shape is metastable and it is interesting to investigate the energy barrier for jumping from one configuration to another. We calculate the energy barrier for SWNT collapse by considering a transition pathway that consists of an initial local deformation that subsequently propagates itself along the SWNT axis. This leads to finite and physically meaningful energy barriers in the limit of infinite nanotubes. Yet, such barriers are surprisingly large (tens of eV) and therefore virtually unsurmountable, which essentially prevents the thermal collapse of a metastable cylindrical at any reasonable temperatures. Moreover, we show that collapse barriers increase counterintuitively with SWNT diameter. Finally, we demonstrate that, despite such huge barriers, SWNTs may collapse relatively easily under external radial forces and we shed light on recent experimental observations of collapsed and cylindrical SWNTs of various diameters.

CARBON 159, 161-165, 2020. DOI: 10.1016/j.carbon.2019.12.030

[P038-2020] "Evaluating viscoelastic properties and membrane electrical charges of red blood cells with optical tweezers and cationic quantum dots - applications to beta-thalassemia intermedia hemoglobinopathy"

Lima, C. N.; Moura, D. S.; Silva, Y. S. S.; Souza, T. H.; Crisafuli, F. A. P.; Silva, D. C. N.; Peres, J. C.; **Cesar, C. L.***; de Araujo, R. E.; Fontes, A.

Biomechanical and electrical properties are important to the performance and survival of red blood cells (RBCs) in the microcirculation. This study proposed and explored methodologies based on optical tweezers and cationic quantum dots (QDs) as biophotonic tools to characterize, in a complementary way, viscoelastic properties and membrane electrical charges of RBCs. The methodologies were applied to normal (HbA) and beta--thalassemia intermedia (Hb beta) RBCs. The beta-thalassemia intermedia disease is a hereditary hemoglobinopathy characterized by a reduction (or absence) of beta-globin chains, which leads to alpha-globin chains precipitation. The apparent elasticity (mu) and membrane viscosity (eta(m)) of RBCs captured by optical tweezers were obtained in just a single experiment. Besides, the membrane electrical charges were evaluated by flow cytometry, exploring electrostatic interactions between cationic QDs, stabilized with cysteamine, with the negatively charged RBC surfaces. Results showed that Hb beta RBCs are less elastic, have a higher eta(m), and presented a reduction in membrane electrical charges, when compared to HbA RBCs. Moreover, the methodologies based on optical tweezers and QDs, here proposed, showed to be capable of providing a deeper and integrated comprehension on RBC rheological and electrical changes, resulting from diverse biological conditions, such as the beta-thalassemia intermedia hemoglobinopathy.

COLLOIDS AND SURFACES B-BIOINTERFACES 186, 110671, 2020. DOI: 10.1016/j.colsurfb.2019.110671

[P039-2020] "Extraction and validation of a new set of CMS pythia8 tunes from underlying-event measurements"

Sirunyany, A. M.; Tumasyan, A.; Adam, W.; **Chinellato, J. A.*; Tonelli Manganote, E. J.***; et al.; CMS Collaboration

New sets of CMS underlying-event parameters ("tunes") are presented for the pythia8 event generator. These tunes use the NNPDF3.1 parton distribution functions (PDFs) at leading (LO), next-to-leading (NLO), or next-to-next-to-leading (NNLO) orders in perturbative quantum chromodynamics, and the strong coupling evolution at LO or NLO. Measurements of charged-particle multiplicity and transverse momentum densities at various hadron collision energies are fit simultaneously to determine the parameters of the tunes. Comparisons of the predictions of the new tunes are provided for observables sensitive to the event shapes at LEP, global underlying event, soft multiparton interactions, and double--parton scattering contributions. In addition, comparisons are made for observables measured in various specific processes, such as multijet, Drell-Yan, and top quark-antiquark pair production including jet substructure observables. The simulation of the underlying event provided by the new tunes is interfaced to a higher-order matrix-element calculation. For the first time, predictions from pythia8 obtained with tunes based on NLO or NNLO PDFs are shown to reliably describe minimum-bias and underlying-event data with a similar level of agreement to predictions from tunes using LO PDF sets.

EUROPEAN PHYSICAL JOURNAL C 80[1], 2020. DOI: 10.1140/epjc/s10052-019-7499-4

[P040-2020] "Few-Wall Carbon Nanotube Coils"

Nakar, D.; Gordeev, G.; Machado, L. D.; Popovitz-Biro, R.; Rechav, K.; **Oliveira, E. F.***; Kusch, P.; Jorio, A.; **Galvao, D. S.***; Reich, S.; Joselevich, E.

While various electronic components based on carbon nanotubes (CNTs) have already been demonstrated, the realization of miniature electromagnetic coils based on CNTs remains a challenge. Coils made of single-wall CNTs with accessible ends for contacting have been recently demonstrated but were found unsuitable to act as electromagnetic coils because of electrical shorting between their turns. Coils made of a few-wall CNT could in principle allow an insulated flow of current and thus be potential candidates for realizing CNT-based electromagnetic coils. However, no such CNT structure has been produced so far. Here, we demonstrate the formation of few-wall CNT coils and characterize their structural, optical, vibrational, and electrical properties using experimental and computational tools. The coils are made of CNTs with 2, 3, or 4 walls. They have accessible ends for electrical contacts and low defect densities. The coil diameters are on the order of one micron, like those of single-wall CNT coils, despite the higher rigidity of few-wall CNTs. Coils with as many as 163 turns were found, with their turns organized in a rippled raft configuration. These coils are promising candidates for a variety of miniature devices based on electromagnetic coils, such as electromagnets, inductors, transformers, and motors. Being chirally and enantiomerically pure few-wall CNT bundles, they are also ideal for fundamental studies of interwall coupling and superconductivity in CNTs.

NANO LETTERS 20[2], 953-962, 2020. DOI: 10.1021/acs.nanolett.9b03977

[P041-2020] "Four-electrodes DBD plasma jet device with additional floating electrode"

do Nascimento, F.*; Machida, M.*; Kostov, K. G.; Moshkalev, S.

A Dielectric Barrier Discharge (DBD) plasma jet in a four electrodes configuration was investigated in order to improve the discharge parameters, such as discharge power and rotational and vibrational temperatures of molecular species in the plasma plume. The improvement attempts were made by introducing an auxiliary floating electrode in a form of a metallic pin inside the DBD device. That piece was placed near the bottom of the main device, centered in relation to the four powered electrodes, which were covered with a dielectric material. By using metallic pins with different lengths, it was observed that there were considerable variations of the plasma parameters as a function of the pin length. Two carrier gases were tested: argon and helium. With helium as the working gas, it was found that there is an optimal pin length that maximizes the plasma power and its vibrational temperature. In addition, it was verified that for the pin of optimum length the relative intensity of light emissions from OH and NO species achieved higher values than in other conditions studied.

EUROPEAN PHYSICAL JOURNAL D 74[1], 14, 2020. DOI: 10.1140/epjd/e2019-100343-9

[P042-2020] "Gluon propagator and three-gluon vertex with dynamical quarks"

Aguilar, A. C.*; De Soto, F.; **Ferreira, M. N.***; Papavassiliou, J.; Rodriguez-Quintero, J.; Zafeiropoulos, S.

We present a detailed analysis of the kinetic and mass terms associated with the Landau gauge gluon propagator in the presence of dynamical quarks, and a comprehensive dynamical study of certain special kinematic limits of the three--gluon vertex. Our approach capitalizes on results from recent lattice simulations with (2+1) domain wall fermions, a novel nonlinear treatment of the gluon mass equation, and the nonperturbative reconstruction of the longitudinal three-gluon vertex from its fundamental Slavnov-Taylor identities. Particular emphasis is placed on the persistence of the suppression displayed by certain combinations of the vertex form factors at intermediate and low momenta, already known from numerous pure Yang-Mills studies. One of our central findings is that the inclusion of dynamical quarks moderates the intensity of this phenomenon only mildly, leaving the asymptotic low-momentum behavior unaltered, but displaces the characteristic "zero crossing" deeper into the infrared region. In addition, the effect of the three-gluon vertex is explored at the level of the effective gauge coupling, whose size is considerably reduced with respect to its counterpart obtained from the ghost-gluon vertex. The main upshot of the above considerations is the further confirmation of the tightly interwoven dynamics between the two- and three-point sectors of QCD.

EUROPEAN PHYSICAL JOURNAL C 80[2], 154, 2020. DOI: 10.1140/epjc/s10052-020-7741-0

[P043-2020] "Hexagonal boron nitride-carbon nanotube hybrid network structure for enhanced thermal, mechanical and electrical properties of polyimide nanocomposites"

Park, O. K.; Owuor, P. S.; **Jaques, Y. M.*; Galvao, D. S.***; Kim, N. H.; Lee, J. H.; Tiwary, C. S.; Ajayan, P. M.

This study suggests the simple and effective synthesis method of chemically interconnected hexagonal boron nitride (h-BN)-carbon nanotubes (CNTs) hybrid materials (BN-Fe-CNT) with aminosilane functionalized iron oxide nanoparticles (NH2-Fe) via amide bond formations. Synthesized BN-Fe-CNT was acting as an effective filler that enhanced the mechanical, thermal, and electrical properties of polyimide (PI) nanocomposites and accelerated polycondensation reaction of poly(amic acid) (PAA) due to its high thermal conductivity and heat diffusivity. At a 2 wt% filler reinforcement, the in-plane thermal conductivity of the BN--Fe-CNT/PI reached 15 W m(-1) K-1 at 200 degrees C, which represents an enhancement of approximately 11430% compared to that of pure PI. Moreover, thermal stability was enhanced from 400 degrees C to 570 degrees C. Furthermore, the connected CNTs between the individual h-BN produced electron pathways through the PI matrix, with the BN-Fe-CNT/PI exhibiting 10(6)times higher electrical conductivity than that of pure PI. The results in this study clearly suggested that the BN-Fe-CNT could be applicable as an effective multi-functional reinforcement in the fabrication of lightweight polymer nanocomposites with superior mechanical properties, high thermal properties, and high electrical conductivities.

COMPOSITES SCIENCE AND TECHNOLOGY 188, 107977, 2020. DOI: 10.1016/j.compscitech.2019.107977

[P044-2020] "High-order dispersion mapping of an optical fiber"

Gil-Molina, A.*; Castaneda, J. A.*; Londono-Giraldo, D. F.; Gabrielli, L. H.; Cardenas, A. M.; **Fragnito, H. L.***

We report on measurements of high-order dispersion maps of an optical fiber, showing how the ratio between the third and fourth-order dispersion (beta(3)/beta(4)) and the zero-dispersion wavelength (lambda(0)) vary along the length of the fiber. Our method is based on Four-Wave Mixing between short pulses derived from an incoherent pump and a weak laser. We find that the variations in the ratio beta(3)/beta(4) are correlated to those in lambda(0). We present also numerical calculations to illustrate the limits on the spatial resolution of the method. Due to the good accuracy in measuring lambda(0) and beta(3)/beta(4) (10(-3) % and 5% relative error, respectively), and its simplicity, the method can be used to identify fiber segments of good uniformity, suitable to build nonlinear optical devices such as parametric amplifiers and frequency comb generators.

OPTICS EXPRESS 28[3], 4258-4273, 2020. DOI: 10.1364/OE.379512

[P045-2020] "Lead Iodide Thin Films via rf Sputtering"

da Silva, J. M. C.*; Borrero, N. F. V.*; Viana, G. A.*; Merlo, R. B.*; Marques, F. C.*

Lead iodide (PbI2) is a precursor for the preparation of the organolead iodide perovskite (CH3NH3PbI3), which has been used in the fabrication of highly efficient solar cells. In this work, a novel route for the deposition of PbI2 thin films is performed by rf sputtering a target made from compressed PbI2 powder. Atomic force microscopy (AFM) and scanning electron microscopy (SEM) revealed that the PbI2 films produced were uniform, pinhole-free, polycrystalline, and had low roughness. A small concentration of Pb nanocrystals observed within the films is attributed to differences in the sputtering yield of lead and iodide from the PbI2 target. A dependence of band gap on rf sputtering power was observed, which was associated with a reduction in the concentration of Pb nanocrystals. The PbI2 films were efficiently converted into CH3NH3PbI3 perovskite films through the immersion into a methylammonium iodide (MAI) solution, which also converted the remaining Pb nanocrystals into perovskite. This methodology has the potential to forge the way toward a new method for the fabrication of large-area perovskite solar cells.

CRYSTAL GROWTH & DESIGN 20[3], 1531-1537, 2020. DOI: 10.1021/acs.cgd.9b01250

[P046-2020] "Measurement of electrons from heavy-flavour hadron decays as a function of multiplicity in p-Pb collisions at root s(NN)=5.02 TeV"

Acharya, S.; Adamova, D.; Adhya, S. P.; **Albuquerque, D. S. D.*; Chinellato, D. D.*; De Souza, R. D.*; Takahashi, J.***; et al.; ALICE Collaboration

The multiplicity dependence of electron production from heavy-flavour hadron decays as a function of transverse momentum was measured in p-Pb collisions at root sNN = 5.02 TeV using the ALICE detector at the LHC. The measurement was performed in the centre-of-mass rapidity interval -1.07 < y(cms)< 0.14 and transverse momentum interval 2 < p(T)< 16 GeV/c. The multiplicity dependence of the production of electrons from heavy-flavour hadron decays was studied by comparing the p(T) spectra measured for different multiplicity classes with those measured in pp collisions (Q(pPb)) and in peripheral p-Pb collisions (Q(cp)). The Q(pPb) results obtained are consistent with unity within uncertainties in the measured p(T) interval and event classes. This indicates that heavy-flavour decay electron production is consistent with binary scaling and independent of the geometry of the collision system. Additionally, the results suggest that cold nuclear matter effects are negligible within uncertainties, in the production of heavy--flavour decay electrons at midrapidity in p-Pb collisions. <g

JOURNAL OF HIGH ENERGY PHYSICS [2], 077, 2020. DOI: 10.1007/JHEP02(2020)077

[P047-2020] "Measurement of Lambda(1520) production in pp collisions at root s=7 TeV and p-Pb collisions at root s(NN)=5.02 TeV"

Acharya, S.; Acosta, F. T.; Adam, J.; **Albuquerque, D. S. D.*; Chinellato, D. D.*; De Souza, R. D.*; Takahashi, J.***; et al.; ALICE Collaboration

The production of the (1520) baryonic resonance has been measured at midrapidity in inelastic pp collisions at v s = 7 TeV and in p-Pb collisions at v sNN = 5.02 TeV for non-single diffractive events and in multiplicity classes. The resonance is reconstructed through its hadronic decay channel (1520). pK- and the charge conjugate with the ALICE detector. The integrated yields and mean transverse momenta are calculated from the measured transverse momentum distributions in pp and p-Pb collisions. The mean transverse momenta follow mass ordering as previously observed for other hyperons in the same collision systems. A Blast-Wave function constrained by other light hadrons (p, K, K0S, p,) describes the shape of the (1520) transverse momentum distribution up to 3.5 GeV/c in p-Pb collisions. In the framework of this model, this observation suggests that the (1520) resonance participates in the same collective radial flow as other light hadrons. The ratio of the yield of (1520) to the yield of the ground state particle remains constant as a function of charged-particle multiplicity, suggesting that there is no net effect of the hadronic phase in p-Pb collisions on the (1520) yield.

EUROPEAN PHYSICAL JOURNAL C 80[2], 160, 2020. DOI: 10.1140/epjc/s10052-020-7687-2

[P048-2020] "Measurement of the top quark pair production cross section in dilepton final states containing one tau lepton in pp collisions at root s=13 TeV"

Sirunyany, A. M.; Tumasyan, A.; Adam, W.; **Chinellato, J. A.*; Tonelli Manganote, E. J.***; et al.; CMS Collaboration

The cross section of top quark pair production is measured in the t (t) over bar -> (lv(l))(tau(h)v(tau))b (b) over bar final state, where tau(h) refers to the hadronic decays of the tau lepton, and l is either an electron or a muon. The data sample corresponds to an integrated luminosity of 35.9 fb(-1) collected in proton-proton collisions at root s = 13TeV with the CMS detector. The measured cross section is sigma(t (t) over bar) = 781 +/- 7 (stat) +/- 62 (syst) +/- 20 (lumi) pb, and the ratio of the partial width Gamma(t -> tau v(tau)b) to the total decay width of the top quark is measured to be 0.1050 +/- 0.0009 (stat) +/- 0.0071 (syst). This is the first measurement of the t (t) over bar production cross section in proton-proton collisions at root s = 13TeV that explicitly includes t leptons. The ratio of the cross sections in the l tau(h) and ll final states yields a value R-l tau h/ll = 0.973 +/- 0.009 (stat) +/- 0.066 (syst), consistent with lepton universality.

JOURNAL OF HIGH ENERGY PHYSICS [2], 191, 2020. DOI: 10.1007/JHEP02(2020)191

[P049-2020] "Measurement of top quark pair production in association with a Z boson in proton-proton collisions at root s = 13 TeV"

Sirunyan, A. M.; Tumasyan, A.; Adam, W.; **Chinellato, J. A.*; Tonelli Manganote, E. J.***; et al.; CMS Collaboration

A measurement of the inclusive cross section of top quark pair production in association with a Z boson using proton-proton collisions at a center-of-mass energy of 13 TeV at the LHC is performed. The data sample corresponds to an integrated luminosity of 77.5 fb(-1), collected by the CMS experiment during 2016 and 2017. The measurement is performed using final states containing three or four charged leptons (electrons or muons), and the Z boson is detected through its decay to an oppositely charged lepton pair. The production cross section is measured to be sigma (tt<mml:mo stretchy="true"><overbar></mml:mover>Z) = 0.95 +/- 0.05 (stat) +/- 0.06 (syst) pb. For the first time, differential cross sections are measured as functions of the transverse momentum of the Z boson and the angular distribution of the negatively charged lepton from the Z boson decay. The most stringent direct limits to date on the anomalous couplings of the top quark to the Z boson are presented, including constraints on the Wilson coefficients in the framework of the standard model effective field theory.

JOURNAL OF HIGH ENERGY PHYSICS [3], 2020. DOI: 10.1007/JHEP03(2020)056

[P050-2020] "Measurements of inclusive jet spectra in pp and central Pb-Pb collisions at root S-NN=5.02 TeV"

Acharya, S.; Adamova, D.; Adler, A.; **Albuquerque, D. S. D.*; Chinellato, D. D.*; Takahashi, J.***; et al.; ALICE Collaboration

This article reports measurements of the p(T)-differential inclusive jet cross section in pp collisions at root S = 5.02 TeV and the p(T)-differential inclusive jet yield in Pb-Pb 0-10% central collisions at root S-NN = 5.02 TeV. Jets were reconstructed at midrapidity with the ALICE tracking detectors and electromagnetic calorimeter using the anti-k(T) algorithm. For pp collisions, we report jet cross sections for jet resolution parameters R = 0.1-0.6 over the range 20 < p(T,jet) < 140 GeV/c, as well as the jet cross-section ratios of different R and comparisons to two next-to-leading-order (NLO)-based theoretical predictions. For Pb-Pb collisions, we report the R = 0.2 and R = 0.4 jet spectra for 40 < p(T,jet) < 140 GeV/c and 60 < p(T,jet) < 140 GeV/c, respectively. The scaled ratio of jet yields observed in Pb-Pb to pp collisions, R-AA, is constructed, and exhibits strong jet quenching and a clear p(T) dependence for R = 0.2. No significant R dependence of the jet R-AA is observed within the uncertainties of the measurement. These results are compared to several theoretical predictions.

PHYSICAL REVIEW C 101[3], 034911, 2020. DOI: 10.1103/PhysRevC.101.034911

[P051-2020] "Measuring momentum-dependent flow fluctuations in heavy-ion collisions"

Hippert, M.*; Chinellato, D. D.*; Luzum, M.; Noronha, J.; da Silva, T. N.; **Tahashi, J.***

In heavy-ion collisions, momentum-dependent pair correlations can be characterized by a principal component analysis (PCA), in which subleading modes are expected to reveal new information on flow fluctuations. However, we find that, as currently measured, these modes can be dominated by multiplicity fluctuations, which serve as an unwanted background. Here, we propose new PCA observables that are robust against multiplicity fluctuations and isolate novel sources of flow fluctuations, thus being suited to provide fresh insight into the initial stages of the system at small length scales.

PHYSICAL REVIEW C 101[3], 034903, 2020. DOI: 10.1103/PhysRevC.101.034903

[P052-2020] "Metallic copper removal optimization from real wastewater using pulsed electrodeposition"

Nepel, T. C. D.; **Landers, R.***; Vieira, M. G. A.; de Almeida Neto, A. F.

The recovery of metals from wastewater is a recurrent problem due to numerous productive activities that produce wastewaters rich in toxic metals. Within this context, this research presents the study and optimization of copper recovery of real wastewater using pulsed electrodeposition. The studied parameters - method, current, temperature, and rotation - influence both the removal of Cu and the composition of the formed deposit, noting that the variation of these parameters enables the removal of copper with formation from crystalline oxides to crystalline copper in its metallic form. The process was optimized, and a 33.59% copper removal from a real wastewater with a deposition efficiency of 84.36% in 30 min was deemed optimal, using fast galvanic pulse, t(on) = 1 ms, 190 mA, 70 rpm, and 37 degrees C. For coating in the optimum point, a metallic and crystalline copper with 100% purity was obtained.

JOURNAL OF HAZARDOUS MATERIALS 384, 121416, 2020. DOI: 10.1016/j.jhazmat.2019.121416

[P053-2020] "Milk fat crystal network as a strategy for delivering vegetable oils high in omega-9,-6, and-3 fatty acids"

Viriato, R. L. S.; Queiros, M. D.; da Silva, M. G.; **Cardoso, L. P.*;** Ribeiro, A. P. B.; Gigante, M. L.

As an alternative to the strategies currently used to deliver unsaturated fatty acids, especially, the essentials omega-6 and 3- fatty acids, the aim of this work was to investigate the effect of the incorporation of 25 e 50% (w/w) of olive, corn and linseed oil into the crystal structure of anhydrous milk fat (AMF). Fatty acid composition, atherogenicity (AI), and thrombogenicity (TI) index, crystallization kinetics, polymorphism by Rietveld method (RM), microstructure, thermal behavior, solid fat content, and lipid compatibility was evaluated. The addition of vegetable oils reduced the saturated fatty acids, and the AI and TI indices of AMF, and increased the concentration of unsaturated, specifically omega-6 and -3 fatty acids. Although vegetable oils caused changes in nucleation and crystallization kinetics, the spherulitic and crystalline morphology and the beta' polymorphism of AMF were maintained. The study demonstrated the possibility of using the crystal structure of AMF as a vehicle for unsaturated fatty acids in food formulations, as an alternative to nutritional supplementation. In addition, studies on the use of RM in blends made with AMF and vegetable oil have not been found in literature, thus demonstrating the relevance of the present study.

FOOD RESEARCH INTERNATIONAL 128, 108780, 2020. DOI: 10.1016/j.foodres.2019.108780

[P054-2020] "Monitoring the dispersion and agglomeration of silver nanoparticles in polymer thin films using localized surface plasmons and Ferrell plasmons"

Hensel, R. C.*; Moreira, M.*; Riul, A.*; Oliveira, O. N.; **Rodrigues, V.*; Hillenkamp, M.***

The ability to disperse metallic nano-objects in a given matrix material is an important issue for the design and fabrication of functional materials. A means to monitor the spatial distribution of the nano-dopants is highly desirable but often possible only a posteriori and with destructive techniques. Here we present a spectroscopic characterization based on different plasmonic responses of silver nanoparticles, their agglomerates, and finally the percolated silver film. We demonstrate its usefulness for the specific case of their dispersion in layer-by-layer polymeric films but the method is extendable to any other host material transparent in the visible/near UV range. Individual silver nanoparticles display the well-known localized surface plasmon resonance around 400nm, which is red-shifted upon inter-particle coupling. The transition regime between weakly coupled particles and fully percolated metal films is, however, much harder to evidence unambiguously. We show here how to monitor this transition using the so-called Ferrell plasmon, a plasmonic mode of the thin film in the mid-UV, and excitable only under oblique irradiation but without specific coupling precautions. We can thus follow the entire transition from isolated to coupled and finally to fully agglomerated nanoparticles by optical spectroscopy.

APPLIED PHYSICS LETTERS 116[10], 103105, 2020. DOI: 10.1063/1.5140247

[P055-2020] "Multiparticle correlation studies in pPb collisions root s(NN)=8.16 TeV"

Sirunyany, A. M.; Tumasyan, A.; Adam, W.; **Chinellato, J. A.*; Tonelli Manganote, E. J.***; et al.; CMS Collaboration

The second- and third-order azimuthal anisotropy Fourier harmonics of charged particles produced in pPb collisions, at root s(NN) = 8.16 TeV, are studied over a wide range of event multiplicities. Multiparticle correlations are used to isolate global properties stemming from the collision overlap geometry. The second-order "elliptic" harmonic moment is obtained with high precision through four-, six-, and eight-particle correlations and, for the first time, the third-order "triangular" harmonic moment is studied using four-particle correlations. A sample of peripheral PbPb collisions at root s(NN) = 5.02 TeV that covers a similar range of event multiplicities as the pPb results is also analyzed. Model calculations of initial-state fluctuations in pPb and PbPb collisions can be directly compared to the high-precision experimental results. This work provides new insight into the fluctuation-driven origin of the v(3) coefficients in pPb and PbPb collisions, and into the dominating overall collision geometry in PbPb collisions at the earliest stages of heavy ion interactions.

PHYSICAL REVIEW C 101[1], 014912, 2020. DOI: 10.1103/PhysRevC.101.014912

[P056-2020] "Multiplicity dependence of (multi-)strange hadron production in proton-proton collisions at root s=13 TeV"

Acharya, S.; Acosta, F. T.; Adam, J.; **Albuquerque, D. S. D.*; Chinellato, D. D.*; De Souza, R. D.*; Takahashi, J.***; et al.; ALICE Collaboration

The production rates and the transverse momentum distribution of strange hadrons at mid-rapidity (vertical bar y vertical bar < 0.5) are measured in proton-proton collisions at root s = 13 TeV as a function of the charged particle multiplicity, using the ALICE detector at the LHC. The production rates of K-S(0), Lambda, Xi, and Omega increase with the multiplicity faster than what is reported for inclusive charged particles. The increase is found to be more pronounced for hadrons with a larger strangeness content. Possible auto-correlations between the charged particles and the strange hadrons are evaluated by measuring the event-activity with charged particle multiplicity estimators covering different pseudorapidity regions. When comparing to lower energy results, the yields of strange hadrons are found to depend only on the mid-rapidity charged particle multiplicity. Several features of the data are reproduced qualitatively by general purpose QCD Monte Carlo models that take into account the effect of densely--packed QCD strings in high multiplicity collisions. However, none of the tested models reproduce the data quantitatively. This work corroborates and extends the ALICE findings on strangeness production in proton-proton collisions at 7 TeV.

EUROPEAN PHYSICAL JOURNAL C 80[2], 167, 2020. DOI: 10.1140/epjc/s10052-020-7673-8

[P057-2020] "Multiscale model of the role of grain boundary structures in the dynamic intergranular failure of polycrystal aggregates"

Galvis, A. F.; **Santos-Florez, P. A.*;** Sollero, P.; **de Koning, M.***; Wrobel, L. C.

A multiscale approach to investigate the influence of the grain boundary (GB) lattice structures on the dynamic intergranular failure in 3D polycrystalline materials is proposed. The model comprises the meso- and atomistic scales using the boundary element method (BEM) and molecular dynamics (MD), respectively. At the mesoscale, stochastic grain morphologies, random crystalline orientations and initial defects are included in the physical model. Moreover, a dynamic high-rate load is imposed to produce dynamic stress and strain waves propagating throughout the polycrystal, inducing the material to be susceptible to fail. The intergranular failure is governed by the critical energy density for shear and cleavage modes, evaluated from a set of nano GBs at the atomistic scale. The novelty is the assessment of the energy density considering its dependency on the interface lattice, leading to a group of failure criteria distributed along the aggregate. The difference in the order of magnitude between these length scales is a challenge for the transition multiscale model. Hence, an asymptotic scaling methodology is adapted for bridging the mechanical strength. Finally, it is worth noting that the level of detail of this criterion, is a remarkable enhancement over other intergranular failure models.

COMPUTER METHODS IN APPLIED MECHANICS AND ENGINEERING 362[SI], 112868 , 2020. DOI: 10.1016/j.cma.2020.112868

[P058-2020] "Possible Quantum Paramagnetism in Compressed Sr2IrO4"

Haskel, D.; Fabbris, G.; Kim, J. H.; **Veiga, L. S. I.*; Mardegan, J. R. L.*;** Escanhoela, C. A., Jr; Chikara, S.; Struzhkin, V.; Senthil, T.; Kim, B. J.; Cao, G.; Kim, J. W.

The effect of compression on the magnetic ground state of Sr2IrO4 is studied with x-ray resonant techniques in the diamond anvil cell. The weak interlayer exchange coupling between square-planar 2D IrO2 layers is readily modified upon compression, with a crossover between magnetic structures around 7 GPa mimicking the effect of an applied magnetic field at ambient pressure. Higher pressures drive an order-disorder magnetic phase transition with no magnetic order detected above 17-20 GPa. The persistence of strong exchange interactions between J(eff) = 1/2 magnetic moments within the insulating IrO2 layers up to at least 35 GPa points to a highly frustrated magnetic state in compressed Sr2IrO4, opening the door for realization of novel quantum paramagnetic phases driven by extended 5d orbitals with entangled spin and orbital degrees of freedom.

PHYSICAL REVIEW LETTERS 124[6], 067201, 2020. DOI: 10.1103/PhysRevLett.124.067201

[P059-2020] "Pseudoscalar glueball mass: a window on three-gluon interactions"

Souza, E. V.*; Ferreira, M. N.*; Aguilar, A. C.*; Papavassiliou, J.; Roberts, C. D.; Xu, S. S.

In pure-glue QCD, gluon-gluon scattering in the J(PC) = 0(-+) channel is described by a very simple equation, especially if one considers just the leading contribution to the scattering kernel. Of all components in this kernel, only the three-gluon vertex, V-mu nu rho, is poorly constrained by contemporary analyses; hence, calculations of 0(-+) glueball properties serve as a clear window onto the character and form of V-mu nu rho. This is important given that many modern calculations of V-mu nu rho predict the appearance of an infrared suppression in the scalar function which comes to modulate the bare vertex after the nonperturbative resummation of interactions. Such behaviour is a peculiar prediction; but we find that the suppression is essential if one is to achieve agreement with lattice-QCD predictions for the 0(-+) glueball mass. Hence, it is likely that this novel feature of V-mu nu rho is real and has observable implications for the spectrum, decays and interactions of all QCD bound-states.

EUROPEAN PHYSICAL JOURNAL A 56[1], 25, 2020. DOI: 10.1140/epja/s10050-020-00041-y

[P060-2020] "Quasar Accretion Disk Sizes from Continuum Reverberation Mapping in the DES Standard-star Fields"

Yu, Z. F.; Martini, P.; Davis, T. M.; **Sobreira, F.*;** et al.

Measurements of the physical properties of accretion disks in active galactic nuclei are important for better understanding the growth and evolution of supermassive black holes. We present the accretion disk sizes of 22 quasars from continuum reverberation mapping with data from the Dark Energy Survey (DES) standard-star fields and the supernova C fields. We construct continuum light curves with the griz photometry that span five seasons of DES observations. These data sample the time variability of the quasars with a cadence as short as 1 day, which corresponds to a rest-frame cadence that is a factor of a few higher than most previous work. We derive time lags between bands with both JAVELIN and the interpolated cross-correlation function method and fit for accretion disk sizes using the JAVELIN thin-disk model. These new measurements include disks around black holes with masses as small as similar to 10(7) M, which have equivalent sizes at 2500 A as small as similar to 0.1 lt-day in the rest frame. We find that most objects have accretion disk sizes consistent with the prediction of the standard thin-disk model when we take disk variability into account. We have also simulated the expected yield of accretion disk measurements under various observational scenarios for the Large Synoptic Survey Telescope Deep Drilling Fields. We find that the number of disk measurements would increase significantly if the default cadence is changed from 3 days to 2 days or 1 day.

ASTROPHYSICAL JOURNAL SUPPLEMENT SERIES 246[1], 16, 2020. DOI: 10.3847/1538-4365/ab5e7a

[P061-2020] "Radiologic evidence that hypothalamic gliosis is improved after bariatric surgery in obese women with type 2 diabetes"

van de Sande-Lee, S.; Melhorn, S. J.; Rachid, B.; Rodovalho, S.; De-Lima, J. C.; Campos, B. M.; Pedro, T.; **Beltramini, G. C.*;** Chaim, E. A.; Pareja, J. C.; Cendes, F.; Maravilla, K. R.; Schur, E. A.; Velloso, L. A.

Background/Objectives Hypothalamic neurons play a major role in the control of body mass. Obese subjects present radiologic signs of gliosis in the hypothalamus, which may reflect the damage or loss of neurons involved in whole-body energy homeostasis. It is currently unknown if hypothalamic gliosis (1) differs between obese nondiabetic (ND) and obese diabetic subjects (T2D) or (2) is modified by extensive body mass reduction via Roux-n-Y gastric bypass (RYGB). Subjects/Methods Fifty-five subjects (all female) including lean controls (CT; n = 13), ND (n = 28), and T2D (n = 14) completed at least one study visit. Subjects underwent anthropometrics and a multi-echo MRI sequence to measure mean bilateral T2 relaxation time in the mediobasal hypothalamus (MBH) and two reference regions (amygdala and putamen). The obese groups underwent RYGB and were re-evaluated 9 months later. Analyses were by linear mixed models. Results Analyses of T2 relaxation time at baseline showed a group by region interaction only in the MBH (P < 0.0001). T2D had longer T2 relaxation times compared to either CT or ND groups. To examine the effects of RYGB on hypothalamic gliosis a three-way (group by region by time) mixed effects model adjusted for age was executed. Group by region (P < 0.0001) and region by time (P = 0.0005) interactions were significant. There was a reduction in MBH relaxation time by RYGB, and, although the T2D group still had higher T2 relaxation time overall compared to the ND group, the T2D group had significantly lower T2 relaxation time after surgery and the ND group showed a trend. The degree of reduction in MBH T2 relaxation time by RYGB was unrelated to clinical outcomes. Conclusion T2 relaxation times, a marker of hypothalamic gliosis, are higher in obese women with T2D and are reduced by RYGB-induced weight loss.

INTERNATIONAL JOURNAL OF OBESITY 44[1], 178-185, 2020. DOI: 10.1038/s41366-019-0399-8

[P062-2020] "Reagentless fabrication of a porous graphene-like electrochemical device from phenolic paper using laser-scribing"

Mendes, L. F.; **de Siervo, A.***; de Araujo, W. R.; Paixao, T. R. L. C.

This study fabricated a portable, high-performance, and reagentless electrochemical devices using CO2 laser-scribing process, which allowed localized carbonization of a non-conductive and low-cost polymer platform, i.e., phenolic-paper. The carbonized material was extensively characterized by Raman spectroscopy, XPS, XRD, SEM, and electrochemical impedance spectroscopy. The carbon-based electrodes were obtained from the photothermal process induced by CO2 laser radiation and subsequently subjected to electrochemical treatment to fabricate a functional material with excellent conductivity and low charge-transfer resistance. Additionally, the laser-scribed electrodes presented a porous structure with graphene-like domains, thus indicating both potential for on-site electroanalytical applications and better performance than conventional carbon electrodes.

CARBON 159, 110-118, 2020. DOI: 10.1016/j.carbon.2019.12.016

[P063-2020] "Scattering Studies with Low-Energy Kaon-Proton Femtoscopy in Proton-Proton Collisions at the LHC"

Acharya, S.; Adamova, D.; Adhya, S. P.; **Albuquerque, D. S. D.*; Chinellato, D. D.*; De Souza, R. D.*; Takahashi, J.***; et al. A Large Ion Collider Expt Collabor

The study of the strength and behavior of the antikaon-nucleon ((K) over bar N) interaction constitutes one of the key focuses of the strangeness sector in low-energy quantum chromodynamics (QCD). In this Letter a unique high-precision measurement of the strong interaction between kaons and protons, close and above the kinematic threshold, is presented. The femtoscopic measurements of the correlation function at low pair-frame relative momentum of (K+ p circle plus K- (p) over bar) and (K- p circle plus K+ (p) over bar) pairs measured in pp collisions at root s = 5, 7, and 13 TeV are reported. A structure observed around a relative momentum of 58 MeV/c in the measured correlation function of (K- p circle plus K+ (p) over bar) with a significance of 4.4 sigma constitutes the first experimental evidence for the opening of the ((K) over bar (0)(n) circle plus K-0 (n) over bar) breaking channel due to the mass difference between charged and neutral kaons. The measured correlation functions have been compared to Julich and Kyoto models in addition to the Coulomb potential. The high-precision data at low relative momenta presented in this work prove femtoscopy to be a powerful complementary tool to scattering experiments and provide new constraints above the (K) over barN threshold for low-energy QCD chiral models.

PHYSICAL REVIEW LETTERS 124[9], 092301, 2020. DOI: 10.1103/PhysRevLett.124.092301

[P064-2020] "Search for a charged Higgs boson decaying into top and bottom quarks in events with electrons or muons in proton-proton collisions at root s=13TeV"

Sirunyany, A. M.; Tumasyan, A.; Adam, W.; **Chinellato, J. A.*; Tonelli Manganote, E. J.***; et al.; CMS Collaboration

A search is presented for a charged Higgs boson heavier than the top quark, produced in association with a top quark, or with a top and a bottom quark, and decaying into a top--bottom quark-antiquark pair. The search is performed using proton-proton collision data collected by the CMS experiment at the LHC at a center-of-mass energy of 13 TeV, corresponding to an integrated luminosity of 35.9 fb(-1). Events are selected by the presence of a single isolated charged lepton (electron or muon) or an opposite-sign dilepton (electron or muon) pair, categorized according to the jet multiplicity and the number of jets identified as originating from b quarks. Multivariate analysis techniques are used to enhance the discrimination between signal and background in each category. The data are compatible with the standard model, and 95% confidence level upper limits of 9.6-0.01 pb are set on the charged Higgs boson production cross section times branching fraction to a top-bottom quark-antiquark pair, for charged Higgs boson mass hypotheses ranging from 200 GeV to 3 TeV. The upper limits are interpreted in different minimal supersymmetric extensions of the standard model.

JOURNAL OF HIGH ENERGY PHYSICS [1], 096, 2020. DOI: 10.1007/JHEP01(2020)096

[P065-2020] "Search for a heavy Higgs boson decaying to a pair of W bosons in proton-proton collisions at root s=13 TeV"

Sirunyan, A. M.; Tumasyan, A.; Adam, W.; **Chinellato, J. A.*; Tonelli Manganote, E. J.*;** et al.; CMS Collaboration

A search for a heavy Higgs boson in the mass range from 0.2 to 3.0 TeV, decaying to a pair of W bosons, is presented. The analysis is based on proton-proton collisions at = 13 TeV recorded by the CMS experiment at the LHC in 2016, corresponding to an integrated luminosity of 35.9 fb(-1).

The W boson pair decays are reconstructed in the 2l2 nu and l nu 2q final states (with l = e or mu). Both gluon fusion and vector boson fusion production of the signal are considered. Interference effects between the signal and background are also taken into account. The observed data are consistent with the standard model (SM) expectation. Combined upper limits at 95% confidence level on the product of the cross section and branching fraction exclude a heavy Higgs boson with SM-like couplings and decays up to 1870 GeV. Exclusion limits are also set in the context of a number of two-Higgs-doublet model formulations, further reducing the allowed parameter space for SM extensions.

JOURNAL OF HIGH ENERGY PHYSICS [3], 34, 2020. DOI: 10.1007/JHEP03(2020)034

[P066-2020] "Search for a heavy pseudoscalar Higgs boson decaying into a 125 GeV Higgs boson and a Z boson in final states with two tau and two light leptons at root s=13 TeV"

Sirunyan, A. M.; Tumasyan, A.; Adam, W.; **Chinellato, J. A.*; Tonelli Manganote, E. J.*;** et al.; CMS Collaboration

A search is performed for a pseudoscalar Higgs boson, A, decaying into a 125 GeV Higgs boson h and a Z boson. The h boson is specifically targeted in its decay into a pair of tau leptons, while the Z boson decays into a pair of electrons or muons. A data sample of proton-proton collisions collected by the CMS experiment at the LHC at root s = 13 TeV is used, corresponding to an integrated luminosity of 35.9 fb(-1). No excess above the standard model background expectations is observed in data. A model-independent upper limit is set on the product of the gluon fusion production cross section for the A boson and the branching fraction to Zh -> ll tau tau. The observed upper limit at 95% confidence level ranges from 27 to 5 fb for A boson masses from 220 to 400 GeV, respectively. The results are used to constrain the extended Higgs sector parameters for two benchmark scenarios of the minimal supersymmetric standard model.

JOURNAL OF HIGH ENERGY PHYSICS [3], 065, 2020. DOI: 10.1007/JHEP03(2020)065

[P067-20202] "Search for dark matter particles produced in association with a Higgs boson in proton-proton collisions at root s=13TeV"

Sirunyan, A. M.; Tumasyan, A.; Adam, W.; **Chinellato, J. A.*; Tonelli Manganote, E. J.***; et al.; CMS Collaboration

A search for dark matter (DM) particles is performed using events with a Higgs boson candidate and large missing transverse momentum. The analysis is based on proton- proton collision data at a center-of-mass energy of 13 TeV collected by the CMS experiment at the LHC in 2016, corresponding to an integrated luminosity of 35.9 fb(-1). The search is performed in five Higgs boson decay channels: h -> b (b) over bar, gamma gamma, tau(+) tau(-), W+W-, and ZZ. The results from the individual channels are combined to maximize the sensitivity of the analysis. No significant excess over the expected standard model background is observed in any of the five channels or in their combination. Limits are set on DM production in the context of two simplified models. The results are also interpreted in terms of a spin-independent DM-nucleon scattering cross section and compared to those from direct-detection DM experiments. This is the first search for DM particles produced in association with a Higgs boson decaying to a pair of W or Z bosons, and the first statistical combination based on five Higgs boson decay channels.

JOURNAL OF HIGH ENERGY PHYSICS [3], 025, 2020. DOI: 10.1007/JHEP03(2020)025

[P068-2020] "Search for electroweak production of a vector-like T quark using fully hadronic final states"

Sirunyany, A. M.; Tumasyan, A.; Adam, W.; **Chinellato, J. A.*; Tonelli Manganote, E. J.***; et al.; CMS Collaboration

A search is performed for electroweak production of a vector--like top quark partner T of charge 2/3 in association with a top or bottom quark, using proton-proton collision data at root s = 13TeV collected by the CMS experiment at the LHC in 2016. The data sample corresponds to an integrated luminosity of 35.9 fb(-1). The search targets T quarks over a wide range of masses and fractional widths, decaying to a top quark and either a Higgs boson or a Z boson in fully hadronic final states. The search is performed using two experimentally distinct signatures that depend on whether or not each quark from the decays of the top quark, Higgs boson, or Z boson produces an individual resolved jet. Jet substructure, b tagging, and kinematic variables are used to identify the top quark and boson jets, and also to suppress the standard model backgrounds. The data are found to be consistent with the expected backgrounds. Upper limits at 95% confidence level are set on the cross sections for T quark-mediated production of tHQq, tZQq, and their sum, where Q is the associated top or bottom heavy quark and q is another associated quark. The limits are given for each search signature for various T quark widths up to 30% of the T quark mass, and are between 2 pb and 20 fb for T quark masses in the range 0.6{2.6TeV. These results are significantly more sensitive than prior searches for electroweak single production of T -> tH and represent the first constraints on T -> tZ using hadronic decays of the Z boson with this production mode.

JOURNAL OF HIGH ENERGY PHYSICS [1], 36, 2020. DOI: 10.1007/JHEP01(2020)036

[P069-2020] "Search for lepton flavour violating decays of a neutral heavy Higgs boson to mu tau and e tau in proton--proton collisions at root s=13 TeV"

Sirunyany, A. M.; Tumasyan, A.; Adam, W.; **Chinellato, J. A.*; Tonelli Manganote, E. J.***; et al.; CMS Collaboration

A search for lepton flavour violating decays of a neutral non--standard-model Higgs boson in the mu tau and e tau decay modes is presented. The search is based on proton-proton collisions at a center of mass energy root s = 13 TeV collected with the CMS detector in 2016, corresponding to an integrated luminosity of 35.9 fb(-1). The tau leptons are reconstructed in the leptonic and hadronic decay modes. No signal is observed in the mass range 200-900 GeV. At 95% confidence level, the observed (expected) upper limits on the production cross section multiplied by the branching fraction vary from 51.9 (57.4) fb to 1.6 (2.1) fb for the mu tau and from 94.1 (91.6) fb to 2.3 (2.3) fb for the e tau decay modes.

JOURNAL OF HIGH ENERGY PHYSICS [3], 103, 2020. DOI: 10.1007/JHEP03(2020)103

[P070-2020] "Search for new neutral Higgs bosons through the H -- ZA -- ` + ` − bb¯ process in pp collisions at √s = 13 TeV"

Sirunyan, A. M.; Tumasyan, A.; Adam, W.; **Chinellato, J. A.*; Tonelli Manganote, E. J.*;** et al.; CMS Collaboration

This paper reports on a search for an extension to the scalar sector of the standard model, where a new CP-even (odd) boson decays to a Z boson and a lighter CP-odd (even) boson, and the latter further decays to a b quark pair. The Z boson is reconstructed via its decays to electron or muon pairs. The analysed data were recorded in proton-proton collisions at a center-of-mass energy <mml:msqrt>s</mml:msqrt> = 13 TeV,

collected by the CMS experiment at the LHC during 2016, corresponding to an integrated luminosity of 35.9 fb(-1). Data and predictions from the standard model are in agreement within the uncertainties. Upper limits at 95% confidence level are set on the production cross section times branching fraction, with masses of the new bosons up to 1000 GeV. The results are interpreted in the context of the two-Higgs-doublet model.

JOURNAL OF HIGH ENERGY PHYSICS [3], 2020. DOI: 10.1007/JHEP03(2020)055

[P071-2020] "Search for physics beyond the standard model in multilepton final states in proton-proton collisions at root s=13 TeV"

Sirunyan, A. M.; Tumasyan, A.; Adam, W.; **Chinellato, J. A.*; Tonelli Manganote, E. J.***; et al.; CMS Collaboration

A search for physics beyond the standard model in events with at least three charged leptons (electrons or muons) is presented. The data sample corresponds to an integrated luminosity of 137 fb(-1) of proton-proton collisions at root s = 13 TeV, collected with the CMS detector at the LHC in 2016-2018. The two targeted signal processes are pair production of type--III seesaw heavy fermions and production of a light scalar or pseudoscalar boson in association with a pair of top quarks. The heavy fermions may be manifested as an excess of events with large values of leptonic transverse momenta or missing transverse momentum. The light scalars or pseudoscalars may create a localized excess in the dilepton mass spectra. The results exclude heavy fermions of the type-III seesaw model for masses below 880 GeV at 95% confidence level in the scenario of equal branching fractions to each lepton flavor. This is the most restrictive limit on the flavor-democratic scenario of the type-III seesaw model to date. Assuming a Yukawa coupling of unit strength to top quarks, branching fractions of new scalar (pseudoscalar) bosons to dielectrons or dimuons above 0.004 (0.03) and 0.04 (0.03) are excluded at 95% confidence level for masses in the range 15-75 and 108-340 GeV, respectively. These are the first limits in these channels on an extension of the standard model with scalar or pseudoscalar particles.

JOURNAL OF HIGH ENERGY PHYSICS [3], 051, 2020. DOI: 10.1007/JHEP03(2020)051

[P072-2020] "Search for production of four top quarks in final states with svame-sign or multiple leptons in proton--proton collisions at root s=13 TeV"

Sirunyany, A. M.; Tumasyan, A.; Adam, W.; **Chinellato, J. A.*; Tonelli Manganote, E. J.***; et al.; CMS Collaboration

The standard model (SM) production of four top quarks (tt over bar tt over ba in proton-proton collisions is studied by the CMS Collaboration. The data sample, collected during the 2016-2018 data taking of the LHC, corresponds to an integrated luminosity of 137fb-1 at a center-of-mass energy of 13TeV. The events are required to contain two same-sign charged leptons (electrons or muons) or at least three leptons, and jets. The observed and expected significances for the tt over bar tt over bar signal are respectively 2.6 and 2.7 standard deviations, and the tt over bar tt over bar cross section is measured to be 12.6-5.2+5.8fb. The results are used to constrain the Yukawa coupling of the top quark to the Higgs boson, yielding a limit of < 1. 7 is the SM value of yt. They are also used to constrain the oblique parameter of the Higgs boson in an effective field theory framework, H.Limits are set on the production of a heavy scalar or pseudoscalar boson in Type--II two-Higgs-doublet and simplified dark matter models, with exclusion limits reaching 350-470GeV and 350-550GeV for scalar and pseudoscalar bosons, respectively. Upper bounds are also set on couplings of the top quark to new light particles.

EUROPEAN PHYSICAL JOURNAL C 80[2], 75. 2020. DOI: 10.1140/epjc/s10052-019-7593-7

[P073-2020] "Search for Supersymmetry with a Compressed Mass Spectrum in Events with a Soft tau Lepton, a Highly Energetic Jet, and Large Missing Transverse Momentum in Proton-Proton Collisions at root s=13 TeV"

Sirunyany, A. M.; Tumasyan, A.; Adam, W.; **Chinellato, J. A.*; Tonelli Manganote, E. J.***; et al.; CMS Collaboration

The first search for supersymmetry in events with an experimental signature of one soft, hadronically decaying tau lepton, one energetic jet from initial-state radiation, and large transverse momentum imbalance is presented. These event signatures are consistent with direct or indirect production of scalar tau leptons ((tau) over tilde) in supersymmetric models that exhibit coannihilation between the (tau) over tilde and the lightest neutralino ((chi) over tilde (0)(1)), and that could generate the observed relic density of dark matter. The data correspond to an integrated luminosity of 77.2 fb(-1) of proton-proton collisions at root s = 13 TeV collected with the CMS detector at the LHC in 2016 and 2017. The results are interpreted in a supersymmetric scenario with a small mass difference (Delta m) between the chargino ((chi) over tilde (+/-)(1)) or next-to-lightest neutralino ((chi) over tilde (0)(2)), and the (chi) over tilde (0)(1). The mass of the (tau) over tilde is assumed to be the average of the (chi) over tilde (1)(+/-) and (chi) over tilde (0)(1) masses. The data are consistent with standard model background predictions. Upper limits at 95% confidence level are set on the sum of the (chi) over tilde (+/-)(1). (chi) over tilde (0)(2), and (tau) over tilde production cross sections for Delta m ((chi) over tilde (+/-)(1),(chi) over tilde (0)(1)) = 50 GeV, resulting in a lower limit of 290 GeVon the mass of the (chi) over tilde (+/-)(1), which is the most stringent to date and surpasses the bounds from the LEP experiments.

PHYSICAL REVIEW LETTERS 124[4], 041803, 2020. DOI: 10.1103/PhysRevLett.124.041803

[P074-2020] "Search for top squark pair production in a final state with two tau leptons in proton-proton collisions at root s=13 TeV"

Sirunyany, A. M.; Tumasyan, A.; Adam, W.; **Chinellato, J. A.*; Tonelli Manganote, E. J.***; et al.; CMS Collaboration

A search for pair production of the supersymmetric partner of the top quark, the top squark, in proton-proton collision events at s = 13 TeV is presented in a final state containing hadronically decaying tau leptons and large missing transverse momentum. This final state is highly sensitive to high-tan beta or higgsino--like scenarios in which decays of electroweak gauginos to tau leptons are dominant. The search uses a data set corresponding to an integrated luminosity of 77.2 fb(-1), which was recorded with the CMS detector during 2016 and 2017. No significant excess is observed with respect to the background prediction. Exclusion limits at 95% confidence level are presented in the top squark and lightest neutralino mass plane within the framework of simplified models, in which top squark masses up to 1100 GeV are excluded for a nearly massless neutralino.

JOURNAL OF HIGH ENERGY PHYSICS [2], 15, 2020. DOI: 10.1007/JHEP02(2020)015

[P075-2020] "Searches for physics beyond the standard model with the MT2 variable in hadronic final states with and without disappearing tracks in proton-proton collisions at s=13Te"

Sirunyany, A. M.; Tumasyan, A.; Adam, W.; **Chinellato, J. A.*; Tonelli Manganote, E. J.***; et al.; CMS Collaboration

Two related searches for phenomena beyond the standard model (BSM) are performed using events with hadronic jets and significant transverse momentum imbalance. The results are based on a sample of proton-proton collisions at a center-of--mass energy of 13Te, collected by the CMS experiment at the LHC in 2016-2018 and corresponding to an integrated luminosity of 137fb-1. The first search is inclusive, based on signal regions defined by the hadronic energy in the event, the jet multiplicity, the number of jets identified as originating from bottom quarks, and the value of the kinematic variable MT2 for events with at least two jets. For events with exactly one jet, the transverse momentum of the jet is used instead. The second search looks in addition for disappearing tracks produced by BSM long-lived charged particles that decay within the volume of the tracking detector. No excess event yield is observed above the predicted standard model background. This is used to constrain a range of BSM models that predict the following: the pair production of gluinos and squarks in the context of supersymmetry models conserving R-parity, with or without intermediate long-lived charginos produced in the decay chain; the resonant production of a colored scalar state decaying to a massive Dirac fermion and a quark; or the pair production of scalar and vector leptoquarks each decaying to a neutrino and a top, bottom, or light-flavor quark. In most of the cases, the results obtained are the most stringent constraints to date.

EUROPEAN PHYSICAL JOURNAL C 80[1], 2020. DOI: 10.1140/epjc/s10052-019-7493-x

[P076-2020] "Spontaneous Symmetry Breaking in Cyclo 18] Carbon"

Pereira, Z. S.; **da Silva, E. Z.***

After the experimental evidence of polyynic as the stable form of cyclo[18]carbon, in the present paper, using ab initio electronic structure calculations, we show that this result is a symmetry breaking event, a consequence of the second-order Jahn-Teller effect. We show that the eigenfunctions associated with lowest unoccupied molecular orbitals (LUMO) and LUMO + 1, the excited states of this ring molecule, interact with the eigenfunctions associated with the ground state (occupied states), and this interaction stabilizes the less symmetric polyynic form of cyclo[18] carbon with D-9h symmetry, instead of the cumulenic form. The frontier state interactions are responsible for the distortions in the symmetry in the electronic structures, lowering the energy and making the polyynic form the stable one with alternating triple and single bonds.

JOURNAL OF PHYSICAL CHEMISTRY A 124[6], SI, 1152-1157, 2020. DOI: 10.1021/acs.jpca.9b11822

[P077-2020] "Studies of J/psi production at forward rapidity in Pb-Pb collisions at root s(NN)=5.02 TeV"

Acharya, S.; Adamova, D.; Adhya, S. P.; **Albuquerque, D. S. D.*; Chinellato, D. D.*; De Souza, R. D.*; Takahashi, J.***; et al.; ALICE Collaboration

The inclusive J/psi production in Pb-Pb collisions at the center--of-mass energy per nucleon pair sNN= 5.02 TeV is presented and compared with previous measurements at sNN = 2.76 TeV as a function of the centrality of the collision, and of the J/psi transverse momentum and rapidity. The inclusive J/psi RAA shows a suppression increasing toward higher transverse momentum, with a steeper dependence for central collisions. The modification of the J/psi average transverse momentum and average squared transverse momentum is also studied. Comparisons with the results of models based on a transport equation and on statistical hadronization are carried out.

JOURNAL OF HIGH ENERGY PHYSICS [2], 41, 2020. DOI: 10.1007/JHEP02(2020)041

[P078-2020] "Sarin and Air Permeation Through a Nanoporous Graphene"

Maria, M. A.*; Fonseca, A. F.*

Sarin gas is a dangerous chemical warfare agent (CWA). It is a nerve agent capable of bringing a person to death in about 15 minutes. A lethal concentration of sarin molecules in air is about 30 mg/m3. Experimental research on this gas requires very careful safety protocols for handling and storage. Therefore, theoretical and computational studies on sarin gas are very welcome and might provide important safe guides towards the management of this lethal substance. In this work, we investigated the interactions between sarin, air and nanoporous graphene, using tools of classical molecular dynamics simulations. Aiming to cast some light in the possible sarin selective filtration by graphene, we designed a bipartite simulation box with a porous graphene nanosheet placed at the middle. Sarin and air molecules were initially placed only on one side of the box so as to create an initial pressure towards the passage of both to the other side. The box dimensions were chosen so that the hole in the graphene was the only possible way through which sarin and air molecules can get to the other side of the box. The number of molecules that passed through the hole in graphene was monitored during 10 ns of simulation and the results for different temperatures were compared. The results show that, as far as the size of the holes are small, van der Waals forces between graphene and the molecules play a significant role on keeping sarin near graphene, at room temperature.

MRS Advances, March 2020. DOI: 10.1557/adv.2020.149

[P079-2020] "Tensions between the appearance data of T2K and NO nu A"

Nizam, M.; Bharti, S.; **Prakash, S.***; Rahaman, U.; Sankar, S. U.

The long baseline neutrino experiments, T2K and NO nu A, have taken significant amount of data in each of the four channels: (a) nu(mu), disappearance, (b) (nu) over bar (mu), disappearance, (c) nu(e) appearance, and (d)(nu) over bar (e) appearance. There is a mild tension between the disappearance and the appearance data sets of T2K. A more serious tension exists between the nu(e) appearance data of T2K and the nu(e)/(nu) over bar (e) appearance data of NO nu A. This tension is significant enough that T2K rules out the best-fit point of NO nu A at 95% confidence level, whereas, NO nu A rules out T2K best-fit point at 90% confidence level. We explain the reason why these tensions arise. We also do a combined fit of T2K and NO nu A data and comment on the results of this fit.

MODERN PHYSICS LETTERS A 35[6], 2050021, 2020. DOI: 10.1142/S0217732320500212

[P080-2020] "Terahertz Hollow Core Antiresonant Fiber with Metamaterial Cladding"

Sultana, J.; Islam, M. S.; **Cordeiro, C. M. B.*;** Dinovitser, A.; Kaushik, M.; Ng, B. W. H.; Abbott, D.

A hollow core antiresonant photonic crystal fiber (HC-ARPCF) with metal inclusions is numerically analyzed for transmission of terahertz (THz) waves.

The propagation of fundamental and higher order modes are investigated and the results are compared with conventional dielectric antiresonant (AR) fiber designs. Simulation results show that broadband terahertz radiation can be guided with six times lower loss in such hollow core fibers with metallic inclusions, compared to tube lattice fiber, covering a single mode bandwidth (BW) of 700 GHz.

FIBERS 8[2], 14, 2020. DOI: 10.3390/fib8020014

[P081-2020] "Trans-Neptunian Objects Found in the First Four Years of the Dark Energy Survey"

Bernardinelli, P. H.; Bernstein, G. M.; Sako, M.; **Sobreira, F.*;** DES Collaboration

We present a catalog of 316 trans-Neptunian bodies (TNOs) detected from the first four seasons ("Y4" data) of the Dark Energy Survey (DES). The survey covers a contiguous 5000 deg(2) of the southern sky in the grizY optical/NIR filter set, with a typical TNO in this part of the sky being targeted by 25-30 Y4 exposures. This paper focuses on the methods used to detect these objects from the 60,000 Y4 exposures, a process made challenging by the absence of the few-hour repeat observations employed by TNO-optimized surveys. Newly developed techniques include: transient/moving object detection by comparison of single-epoch catalogs to catalogs of "stacked" images; quantified astrometric error from atmospheric turbulence; new software for detecting TNO linkages in a temporally sparse transient catalog, and for estimating the rate of spurious linkages; use of faint stars to determine the detection efficiency versus magnitude in all exposures. Final validation of the reality of linked orbits uses a new "sub-threshold confirmation" test, wherein we demand the object be detectable in a stack of the exposures in which the orbit indicates an object should be present, but was not individually detected. This catalog contains all validated TNOs which were detected on >= 6 unique nights in the Y4 data, and is complete to r less than or similar to 23.3 mag with virtually no dependence on orbital properties for bound TNOs at distance 30 au d < 2500 au. The catalog includes 245 discoveries by DES, 139 not previously published. The final DES TNO catalog is expected to yield >0.3 mag more depth, and arcs of >4 yr for nearly all detections.

ASTROPHYSICAL JOURNAL SUPPLEMENT SERIES 247[1], 32, 2020. DOI: 10.3847/1538-4365/ab6bd8

[P082-2020] "Tunable localized surface plasmon graphene metasurface for multiband superabsorption and terahertz sensing"

Islam, M. S.; Sultana, J.; Biabanifard, M.; Vafapour, Z.; Nine, M. J.; Dinovitser, A.; **Cordeiro, C. M. B.*;** Ng, B. W. H.; Abbott, D.

We propose a plasmon induced tunable metasurface for multiband superabsorption and terahertz sensing. It consists of a graphene sheet that facilitates perfect absorption where the graphene pattern at the top layer creates an enhanced evanescent wave that facilitates the metasurface to work as a sensor. The modelling and numerical analysis are carried out using Finite Element Method (FEM) based software, CST microwave studio where a genetic algorithm (GA) is used to optimize the geometric parameters, and metasurface tunability is achieved via an external gate voltage on the graphene. By exploiting graphene's tunable properties we demonstrate a multiband superabsorption spectra having a maximum absorption of 99.7% in a frequency range of 0.1-2.0 THz that also maintain unique optical performance over a wide incidence angle. Further results show how the superabsorber can be used as a sensor, where the resonance frequency shifts with the refractive index of the surrounding environment.

CARBON 158, 559-567, 2020. DOI: 10.1016/j.carbon.2019.11.026

[P083-2020] "Validation of a Multifocal Segmentation Method for Measuring Metabolic Tumor Volume in Hodgkin Lymphoma"

Camacho, M. R.; Etchebehere, E.; Tardelli, N.; Delamain, M. T.; Vercosa, A. F. A.; **Takahashi, M. E. S.*;** Brunetto, S. Q.; Metze, I. G. H. L.; Souza, C. A.; Cerci, J. J.; Ramos, C. D.

Quantification of metabolic tumor volume (MTV) and total lesion glycolysis (TLG) can be time-consuming. We evaluated the performance of an automatic multifocal segmentation (MFS) method of quantification in patients with different stages of Hodgkin lymphoma, using the multiple VOI (MV) method as reference.Methods: This prospective bicentric study included 50 patients with Hodgkin lymphoma who underwent staging F-18-FGD PET/CT. The examinations were centrally reviewed and processed with commercial MFS software to obtain MTV and TLG using 2 fixed relative thresholds (40% and 20% of SUV max) for each lesion. All PET/CT scans were processed using the MV and MFS methods. Interclass correlation coefficients and Bland-Altman plots were used for statistical analysis. Repeated calculations of MW and TLG values by 2 observers with different degrees of PET/CT imaging experience were used to ascertain interobserver agreement on the MFS method. Results: The means and SDs obtained for the MW with MV and MFS were, respectively, 736 +/- 856 mL and 660 +/- 699 mL for the 20% threshold and 313 +/- 359 mL and 372 +/- 434 mL for the 40% threshold. The time spent calculating the MW was much shorter with the MFS method than with the MV method (median time, 11.6 min [range, 1-30 min] and 64.4 min [range, 1-240 min], respectively), especially in patients with advanced disease. Time spent was similar in patients with localized disease. There were no statistical differences between the MFS values obtained by the 2 different observers. Conclusion: MTV and TLG calculations using MFS are reproducible, generate similar results to those obtained with MV, and are much less timing-consuming. Main differences between the 2 methods were related to difficulties in avoiding overlay of VOIs in the MV technique. MV and MFS perform equally well in patients with a small number of lesions.

JOURNAL OF NUCLEAR MEDICINE TECHNOLOGY 48[1], 30-35, 2020. DOI: 10.2967/jnmt.119.231118

[P084-2020] "Waste Tire Rubber-based Refrigerants for Solid-state Cooling Devices"

Bom, N. M.; Usuda, E. O.; **Gigliotti, M. D.*;** de Aguiar, D. J. M.; Imamura, W.; **Paixao, L. S.*;** Carvalho, A. M. G.

Management of discarded tires is a compelling environmental issue worldwide. Although there are several approaches developed to recycle waste tire rubbers, their application in solid-state cooling is still unexplored. Considering the high barocaloric potential verified for elastomers, the use of waste tire rubber (WTR) as a refrigerant in solid-state cooling devices is very promising. Herein, we investigated the barocaloric effects in WTR and polymer blends made of vulcanized natural rubber (VNR) and WTR, to evaluate its feasibility for solid-state cooling technologies. The adiabatic temperature changes and the isothermal entropy changes reach giant values, as well as the performance parameters, being comparable or even better than most barocaloric materials in literature. Moreover, pure WTR and WTR-based samples also present a faster thermal exchange than VNR, consisting of an additional advantage of using these discarded materials. Thus, the present findings evidence the encouraging perspectives of employing waste rubbers in solid-state cooling based on barocaloric effects, contributing to both the recycling of polymers and the sustainable energy technology field.

CHINESE JOURNAL OF POLYMER SCIENCE, 2020. DOI: 10.1007/s10118-020-2385-y

Eventos publicados 2019

[P001-2019] "Archaeological mirrors of Central and South America"

Lunazzi, J. J.*

It is not commonly known that the first mirrors with high quality of imaging corresponds to the continent mostly known as "The Americas", but the fact is that in Central and South America some civilizations employed high quality mirrors and its images can be considered almost as perfect as those of our ordinary actual mirrors. This knowledge belonged exclusively to archaeologists until it was started to be included in research of the optics community. Not many, but interesting papers were published in the following years and a first book on the subject was published. The references to the subject are increasing and it is clear that there is still work to do to get a better knowledge on how the mirrors were made and employed, in particular, for the South American civilizations. Because we employ mirrors in many different situations at the laboratory, we can contribute to better understanding its ancient use in the times of its invention. This presentations is a claim for more work to be done envolving physicists and archaeologists working together.

Proceedings of X Iberoamerican Optics Meeting XIII Latinamerican Meeting on Optics, Lasers and Applications -Mexican Optics and Photonics Meeting 2019, RIAO-OPTILAS-MOPM 2019, Cancún, Quintana Roo, México, September 23-27, 2019. Acesso: https://www.riao.org.mx/optilas_2019/archivos/Proceedings_RIAO_OPTILAS_MOPM_2019.pdf

[P002-2019] "Wavelength encoding of depth revealed"

Lunazzi, J. J.*

Initiated in 1984 after seeing the photographic reproduction of a hologram, already in the year 1988 the idea that a hologram encodes all the information of depth of its image was demonstrated and soon the idea was extended to the spectral coding of a diffraction grating. Both discoveries were published in 1990. More recently, a simplified explanation was made of both cases, including better photographs that avoids the problem of wavelength representation in printed color images. Although very evident when comparing both processes that the main element acting is the different path of rays exiting from any image point to the final image being a wavelength property, only after this new reviewing of the two processes was that I noticed its generality and extended it to refraction, something that could have been easily discovered by many others when manipulating refraction experiments.

Proceedings of X Iberoamerican Optics Meeting XIII Latinamerican Meeting on Optics, Lasers and Applications -Mexican Optics and Photonics Meeting 2019, RIAO-OPTILAS-MOPM 2019, Cancún, Quintana Roo, México, September 23-27, 2019. Acesso: https://www.riao.org.mx/optilas_2019/archivos/Proceedings_RIAO_OPTILAS_MOPM_2019.pdf

***Autores da comunidade IFGW**
Fonte: Web of Science on-line (WOS)

Defesas de Dissertações do IFGW

[D003-2020] "Estudo de materiais funcionais através de técnicas avançadas de luz síncrotron correlacionadas"
Aluno: Francisco Mateus Cirilo da Silva
Orientador: Prof. Dr. Helio Cesar Nogueira Tolentino
Data: 22/04/2020

[D004-2020] "Acoplamento Josephson negativo em junções a base de semimetais topológicos"
Aluno: Carlos Alberto Invernizzi Canhassi
Orientador: Prof. Dr. Iakov Veniaminovitch Kopelevitch
Data: 30/04/2020

[D005-2020] "Modelagem teórica de monocamadas anfifílicas : gás de rede de Doniach em redes bipartidas na aproximação de campo médio"
Aluno: Carolina Paz Barateiro Vignoto
Orientador: Prof. Dr. Mário Noboru Tamashiro
Data: 11/05/2020

[D006-2020] "Manipulação da Orientação de Spins em Filmes Finos Antiferromagnéticos de CoO por Deformações Estruturais"
Aluno: Marina Raboni Ferreira
Orientador: Prof. Dr. Márcio Medeiros Soares
Data: 12/05/2020

Defesas de Teses do IFGW

[T003-2020] "Sincronização induzida por forças externas em redes modulares"
Aluno: Carolina Arruda Moreira
Orientador: Prof. Dr. Marcus Aloizio Martinez de Aguiar
Data: 19/03/2020

[T004-2020] "Nanofios Semicondutores III-V baseados em Ga: Crescimento, Novos Catalisadores e Propriedades Ópticas"
Aluno: Bruno César da Silva
Orientador: Profa. Dra. Mônica Alonso Cotta
Data: 27/03/2020

[T005-2020] "Aplicações de nanofios semicondutores para a investigação do efeito da N-Acetilcisteína na bactéria Xylella fastidiosa"
Aluno: Aldeliane Maria da Silva
Orientador: Profa. Dra. Mônica Alonso Cotta
Data: 30/04/2020

[T006-2020] "Cálculo de Propriedades Térmicas utilizando Simulação Molecular"
Aluno: Rodolfo Paula Leite
Orientador: Prof. Dr. Maurice de Koning
Data: 08/05/2020

Fonte: Portal IFGW/Pós-graduação - Agenda de Colóquios, Defesas e Seminários.
Disponível em: http://portal.ifi.unicamp.br/pos-graduacao

Defesas de Teses e Dissertações do PECIM

[P001-2020] "Gamificação no Ensino de Matemática com Jogos de Escape Room e RPG: Percepções sobre suas Contribuições e Dificuldades"
Aluno: Mariana Maria Rodrigues Aiub
Orientador: Profa. Dra. Miriam Cardoso Utsumi
Data: 01/04/2020

Fonte: Página do PECIM - Programa de Pós-Graduação Multiunidades em Ensino de Ciências e Matemática – Mestrado e Doutorado (PECIM) da Unicamp.
Disponível em: https://www.pecim.unicamp.br/bancas

Fique em Casa!

Desde fevereiro de 2020 o
Boletim Abstracta está em novo endereço web:

<https://econtents.bc.unicamp.br/boletins/index.php/abstracta>

Abstracta

Instituto de Física
Diretor: Prof. Dr. Pascoal José Giglio Pagliuso
Diretora Associada: Profa. Dra. Mônica Alonso Cotta
Universidade Estadual de Campinas - UNICAMP
Cidade Universitária Zeferino Vaz
13083-859 - Campinas - SP - Brasil
e-mail: secdir@ifi.unicamp.br
Fone: +55 19 3521-5300

Publicação

Biblioteca do Instituto de Física Gleb Wataghin
http://portal.ifi.unicamp.br/biblioteca

Diretora Técnica: Sandra Maria Carlos Cartaxo
Coordenadora da Comissão de Biblioteca: Profa. Dra. Arlene Cristina Aguilar

Elaboração:
Maria Graciele Trevisan (Bibliotecária)
Ayres Neri da Cunha Junior (Técnico Administrativo)
contato: infobif@ifi.unicamp.br